ADVANCES IN ATMOSPHERIC SCIENCES, VOL. 39, AUGUST 2022, 1271–1284

• **Original Paper** •

The Variability of Air-sea O_2 Flux in CMIP6: Implications for Estimating Terrestrial and Oceanic Carbon Sinks※

Changyu LI[1], Jianping HUANG*[2], Lei DING[1], Yu REN[1], Linli AN[1], Xiaoyue LIU[1], and Jiping HUANG[3]

[1]*College of Atmospheric Sciences*, *Lanzhou University*, *Lanzhou* 730000, *China*

[2]*Collaborative Innovation Center for Western Ecological Safety*, *Lanzhou University*, *Lanzhou* 730000, *China*

[3]*Enlightening Bioscience Research Center*, *Mississauga*, *L4X* 2X7, *Canada*

(Received 27 July 2021; revised 24 September 2021; accepted 8 October 2021)

ABSTRACT

The measurement of atmospheric O_2 concentrations and related oxygen budget have been used to estimate terrestrial and oceanic carbon uptake. However, a discrepancy remains in assessments of O_2 exchange between ocean and atmosphere (i.e. air-sea O_2 flux), which is one of the major contributors to uncertainties in the O_2-based estimations of the carbon uptake. Here, we explore the variability of air-sea O_2 flux with the use of outputs from Coupled Model Intercomparison Project phase 6 (CMIP6). The simulated air-sea O_2 flux exhibits an obvious warming-induced upward trend (~1.49 Tmol yr^{-2}) since the mid-1980s, accompanied by a strong decadal variability dominated by oceanic climate modes. We subsequently revise the O_2-based carbon uptakes in response to this changing air-sea O_2 flux. Our results show that, for the 1990–2000 period, the averaged net ocean and land sinks are 2.10±0.43 and 1.14±0.52 GtC yr^{-1} respectively, overall consistent with estimates derived by the Global Carbon Project (GCP). An enhanced carbon uptake is found in both land and ocean after year 2000, reflecting the modification of carbon cycle under human activities. Results derived from CMIP5 simulations also investigated in the study allow for comparisons from which we can see the vital importance of oxygen dataset on carbon uptake estimations.

Key words: air-sea O_2 flux, carbon budget, land and ocean carbon sinks, CMIP6

Citation: Li, C. Y., J. P. Huang, L. Ding, Y. Ren, L. L. An, X. Y. Liu, and J. P. Huang, 2022: The variability of air-sea O_2 flux in CMIP6: Implications for estimating terrestrial and oceanic carbon sinks. *Adv. Atmos. Sci.*, **39**(8), 1271−1284, https://doi.org/10.1007/s00376-021-1273-x.

Article Highlights:

- CMIP6 outputs are used to systematically analyze the characteristics of air-sea O_2 flux under climate change.
- The study provides a valuable complement for global carbon sinks based on the tight relationship between oxygen and carbon cycle.
- The vital role of oceanic oxygen outgassing in O_2-based estimations of land and ocean carbon uptake is revealed in this study.

1. Introduction

Human beings are now faced with continuous growth of the climate risk in the warming world. The climate change, occurring mainly as a consequence of anthropogenic CO_2 emissions, is already wielding its influences on ecosystems, economic sectors and people's health (Bopp et al., 2013; Huang et al., 2016; Frölicher et al., 2018; Wei et al., 2021). An increasing number of evidence warns us that actions should be taken urgently to minimize dangerous anthropogenic interference with the climate system, limiting global warming to 2 degrees – a threshold laid down by the Paris Agreement (Seneviratne et al., 2016; Huang et al., 2017b). Under this circumstance, the carbon neutrality, which refers to the balance of emissions of carbon dioxide with its removal, has become one of the most essential things human society needs to achieve in the mid-late 21st century (Dhanda and Hartman, 2011; Niu et al., 2021).

The land and ocean play an important role in the storage of atmospheric CO_2 (Dai et al., 2013; DeVries et al., 2019). It has been reported that the land and ocean have sequestered approximately half of the anthropogenic CO_2

※ This paper is a contribution to the special issue on Carbon Neutrality: Important Roles of Renewable Energies, Carbon Sinks, NETs, and non-CO_2 GHGs.

* Corresponding author: Jianping HUANG
Email: hjp@lzu.edu.cn

emitted to the atmosphere in the past decades, which helps greatly buffer climate change (Friedlingstein et al., 2019; Gao et al., 2019, 2020). Thus, for a reasonable design of global warming mitigation and carbon neutrality strategies, there is a pressing need to address the effectiveness of terrestrial and oceanic carbon uptake and their susceptibility to climate change. According to this view, the measurement of atmospheric O_2 concentrations and related oxygen budget could provide us a concise and effective method to estimate carbon-uptake capacity of land and ocean on the basis of the close relationship between oxygen and carbon (Huang et al., 2018, 2021; Han et al., 2021; Li et al., 2021).

The accuracy of this O_2-based carbon uptake estimation largely depends on how the oxygen data, especially the air-sea O_2 exchange, is processed in the calculation. Early studies used to assume that there was no long-term oceanic effect of O_2 on the atmosphere (Keeling and Shertz, 1992; Battle et al., 2000). However, a number of indications have revealed the huge oceanic heat uptake under climate change (Willis et al., 2004; Cheng et al., 2018; Cheng and Zhu, 2018; Li et al., 2019), which implies the air-sea O_2 exchange could vary as a consequence of warming-induced solubility and circulation changes (Bopp et al., 2002; Li et al., 2020). Later studies have thus taken air-sea O_2 flux into consideration (Manning and Keeling, 2006; Tohjima et al., 2019), where the oceanic O_2 outgassing to the atmosphere is approximately estimated by a linear regression with ocean heat content, assuming the relationship between gas flux and heat flux bears a proportional relationship at the air–sea interface. In fact, mechanisms that control the variability of air-sea O_2 flux are rather complicated. Its temporal and spatial variations could be affected by changes in ocean primary production, ventilation and stratification, as well as oceanic internal modes such as El Niño-Southern Oscillation(ENSO) (Resplandy et al., 2015; Yang et al., 2017). The intensified ocean heat uptake in the past few decades (Trenberth et al., 2014; Cheng et al., 2017) also wields its influences in the long-term period. How to accurately quantify the air-sea O_2 flux has therefore been one of the most important questions in the field of O_2-based carbon uptake estimations.

Here, based on recent CMIP6 model simulations, we systematically investigate the characteristics of air-sea O_2 flux and from it, we subsequently calculate the terrestrial and oceanic carbon sinks. We hope to provide a better understanding of air-sea O_2 flux under ongoing climate change. We also hope the applications of process-based air-sea O_2 flux from CMIP6 model simulations can provide a more comprehensive and reliable carbon sink estimation, compared with results from previous studies where the air-sea O_2 flux is not considered or simply approximated by a linear relationship between O_2 outgassing and heat content.

The paper is arranged as follows. Section 2 describes the detailed method of O_2-based carbon sink estimations and the datasets, especially air-sea O_2 flux, used in this study. The climatology characteristics of air-sea O_2 flux and its variability under climate change in CMIP6 are shown in section 3.1. Section 3.2 provides our estimations of terrestrial and oceanic carbon sinks with the use of this air-sea O_2 flux. Discussion and conclusion are presented in section 4.

2. Data and methods

2.1. *O_2-based estimations of terrestrial and oceanic carbon sinks*

2.1.1. *Mass balanced equations for global oxygen and carbon budgets*

The assessments of land and ocean carbon sinks in this study are based on the strong relationship between oxygen and carbon, which can be written as follows (Keeling and Manning, 2014; Li et al., 2021):

$$\Delta CO_2 = F_{\text{fossil}} - S_{\text{ocean}} - S_{\text{land}} \,, \tag{1}$$

$$\Delta O_2 = -\alpha_F F_{\text{fossil}} + \alpha_B S_{\text{land}} + F_{\text{air-sea}} \,, \tag{2}$$

where ΔCO_2 and ΔO_2 represent changes in atmospheric CO_2 and O_2; F_{fossil} is the industrial CO_2 emissions, which mainly comes from fossil fuel combustion; $F_{\text{air-sea}}$ represents the air-sea O_2 flux; α_F and α_B are dimensionless parameters which represent the globally averaged O_2: CO_2 mole exchange ratios for fossil fuel burning and biological process; S_{land} and S_{ocean} represent the net land carbon sink and ocean carbon sink, respectively. These two equations briefly describe the human impacts on the oxygen and carbon cycles. All variables in the equations mentioned above use the units of mole.

2.1.2. *Observed atmospheric CO_2 and O_2 concentrations*

The concentrations of CO_2 in the atmosphere (X_{CO_2}) are measured using the unit of "ppm" (parts per million). Its change can be expressed as

$$\Delta X_{CO_2} = \frac{\Delta CO_2}{M_{\text{air}}} \,, \tag{3}$$

where M_{air} represents the global total number of moles of dry air (M_{air}=1.769×10^{20}). The change of atmospheric O_2 concentrations, however, is typically measured as the mole ratio changes of O_2/N_2 rather than the mole fraction such as ppm, due to its high abundance in the atmosphere. Following Keeling and Shertz (1992), the O_2 content of an air sample can be defined as

$$\delta(O_2/N_2) = \frac{(O_2/N_2)_{\text{sample}} - (O_2/N_2)_{\text{ref}}}{(O_2/N_2)_{\text{ref}}} \,, \tag{4}$$

where $(O_2/N_2)_{\text{sample}}$ is the mole ratio of O_2 to N_2 in the sample air and $(O_2/N_2)_{\text{ref}}$ is the ratio in an arbitrary reference gas. Note that $\delta(O_2/N_2)$ is typically multiplied by 10^6 and expressed as "per meg" unit. The observed changes of $\delta(O_2/N_2)$ in the atmosphere could thus be written as

$$\Delta(\delta(O_2/N_2)) = \left(\frac{\Delta O_2}{X_{O_2}} - \frac{\Delta N_2}{X_{N_2}}\right)\frac{1}{M_{\text{air}}} \,, \tag{5}$$

where ΔO_2 and ΔN_2 are changes in moles of atmospheric O_2

and N_2; X_{O_2} and X_{N_2} are the standard mole fraction of O_2 and N_2 in the atmosphere (X_{O_2} = 0.2094 and X_{N_2} = 0.7808).

According to Eqs. (1)–(5), the land and ocean carbon sink can be written as

$$B = \frac{1}{\alpha_B}\left[\Delta(\delta(O_2/N_2))M_{air}X_{O_2} + \alpha_F F_{fossil} - F_{eff}\right], \quad (6)$$

$$O = \frac{1}{\alpha_B}\left[(\alpha_B - \alpha_F)F_{fossil} - \left(\Delta(\delta(O_2/N_2))X_{O_2} + \alpha_B \Delta X_{CO_2}\right)M_{air} + F_{eff}\right], \quad (7)$$

$$F_{eff} = F_{air-sea} - \frac{X_{O_2}}{X_{N_2}}\Delta N_2\,. \quad (8)$$

The observed timeseries of atmospheric CO_2 and O_2 concentrations [i.e. X_{CO_2} and $\delta(O_2/N_2)$] can be downloaded from Scripps O_2 Program (https://scrippso2.ucsd.edu/), which provides records of both CO_2 and O_2 concentrations at 12 stations. In this study, we choose the longest three timeseries, at Alert (82.5°N, 62.3°W), La Jolla (32.9°N, 277.3° W), and Cape Grim (40.7°S, 144.7°E), respectively, and calculate the average with weights of 0.25, 0.25, 0.5 (given the equal weight in both hemispheres).

2.1.3. *Global fossil-fuel combustion and the oxidative ratio*

The global CO_2 emissions (F_{fossil}) are derived from Carbon Dioxide Information Analysis Center (CDIAC, Andres et al., 2016), which counts the consumptions of each type of fossil fuel. It should be noted that each fuel type has its own combustion ratio (α_F), as shown in Table 1 (Liu et al., 2020). The global averaged α_F therefore slightly varies with time due to changes of global energy sources [Fig. S1 in the Electronic Supplementary Material, (ESM)]. The oxidative ratio α_B also exhibits temporal variations due to modifications to global vegetation cover by human activities, however, it is generally believed the decrease of α_B is less than 0.01 over 100 years (Randerson et al., 2006). We thus set the typical value of α_B as 1.10 according to previous studies (Keeling and Manning, 2014; Battle et al., 2019).

2.2. *The air-sea O_2 flux*

Due to the importance of O_2 flux ($F_{air\text{-}sea}$) in estimating the carbon uptake, here we discuss it in greater detail. The air-sea O_2 flux evaluated in this study builds on the process-based ocean physical and biochemical models developed as part of Coupled Model Intercomparison Project phase 6 (CMIP6), which can be downloaded from https://esgf-node.llnl.gov/search/cmip6/. The detailed descriptions of these models are presented in Table 2. Here we choose the historical experiments of these models to match the timeseries of O_2 observations. Note that the air-sea O_2 flux is calculated by the model in mol m^{-2} s^{-1}, so we convert to mol of oxygen per year (mol m^{-2} yr^{-1}). For sake of comparisons and analysis, all the model results are gridded to 1°×1° resolution.

Furthermore, it should be noted that, due to import of N_2 in the atmospheric O_2 observations, oceanic N_2 outgassing must be considered in the calculations. The total effect of the ocean on carbon sinks could thus be expressed as Eq. (8). Here we apply the tuning parameter β=0.88 to represent the negative effect of N_2 outgassing (Keeling and Manning, 2014); it can be shown that the equation can be written as

$$F_{eff} = \beta F_{air-sea}\,. \quad (9)$$

The related ocean physics variables such as sea temperature, salinity, and mixed layer depth in CMIP6 are also used in this study to analyze mechanisms of O_2 flux change.

2.3. *The EEMD method*

We use the ensemble empirical mode decomposition (EEMD) method to separate the human-induced long-term signals from natural decadal variability in the time series of air-sea O_2 flux. This noise-assisted method can separates scales naturally without any prior subjective criterion (Ji et al., 2014; Huang et al., 2017a). EEMD performs operations that partition a series into different "modes" (Intrinsic Mode Functions, IMFs), which are expressed by the following equation:

Table 1. Typical oxidative ratio for each fuel type.

Fuel Type	Oxidative ratio (α_F)
Solid fuel (coal)	1.17±0.03
Liquid fuel (oil)	1.44±0.03
Gas fuel (natural gas)	1.95±0.04
Cement production	0.00±0.00
Biofuel	1.07±0.03

Table 2. The CMIP6 models used in this study to obtain the air-sea O_2 flux[a].

Model Name	Institute
IPSL-CM5A2-INCA	Institut Pierre-Simon Laplace, France
GFDL-CM4	Geophysical Fluid Dynamics Laboratory, USA
GFDL-ESM4	Geophysical Fluid Dynamics Laboratory, USA
MPI-ESM-1-2-HAM	Max Planck Institute for Meteorology, Germany
NorESM2-LM	Norwegian Climate Centre, Norway
NorESM2-MM	Norwegian Climate Centre, Norway

[a] The air-sea O_2 flux was calculated by the model in mol m^{-2} s^{-1}, so we converted this value to mol of oxygen per year by converting from seconds to year (×31 536 000).

$$X(t) = \sum_{i=1}^{n} \mathrm{IMF}_i(t) + r_n(t) \ , \tag{10}$$

where $\mathrm{IMF}_i(t)$ is the ith IMF, and $r_n(t)$ is the residual of data $X(t)$. The detailed descriptions of the steps on how to execute EEMD method can be found in Text S1 in the ESM. In this study, the noise added to the data has an amplitude that is 0.2 times the standard deviation of the raw data, and the ensemble number is 400. The number of IMFs is 6. A python version of EEMD is available at https://www.github.com/laszukdawid/PyEMD (Laszuk, 2017).

3. Results

3.1. *The characteristics of air-sea O_2 exchange in CMIP6*

3.1.1. *Climatological status of air-sea O_2 flux in 1985–2014 and evaluation against available studies*

The transfer of gases across the air-sea interface is controlled by several physical, biological and chemical processes in the atmosphere and ocean, which could influence not only the partial pressure differences but also the efficiency of transfer processes (Wanninkhof, 1992; Liang et al., 2013). The air-sea O_2 flux thus varies considerably among the ocean regions. Figure 1a presents the model-ensemble-mean of annual air-sea O_2 flux averaged from 1985 to 2014 in CMIP6 historical experiments (positive means a flux to the atmosphere). Spatial distributions of O_2 flux in each individual model can be found in Fig. S2 in the ESM. The results show an overall net O_2 outgassing from ocean to the atmosphere at low latitudes, while a significant influx of O_2 occurs at high latitudes. The tropical and subtropical ocean (30°S–30°N) emits approximately 250.8±38.4 Tmol O_2 per year (1 Tmol = 10^{12} mol), which is partly compensated by O_2 absorption in the high-latitude ocean, about −105.2±24.8 and −87.2±41.4 Tmol yr^{-1} in the Northern (>30°N) and Southern Hemisphere (>30°S), respectively, eventually leading to a net O_2 outgassing of ~58.5±9.6 Tmol yr^{-1} over the global ocean. This pattern highlights the solubility effect driven by meridional temperature gradients, as well as combinations of the dynamical and biological effects, which lead to a surplus of oceanic O_2 production in low latitudes (Bopp et al., 2002).

Furthermore, the simulated O_2 flux is evaluated against results derived from previous studies (Gruber et al., 2001; Resplandy et al., 2015), which are found in Fig. 1b . The ocean is divided into 13 regions for sake of comparison (Fig. S3 in the ESM). The patterns presented by the ensemble-mean of the suite of models in CMIP6 correspond well with estimations based on ocean inversions (Gruber et al., 2001), except for the Sothern Ocean. The results derived from Gruber et al. (2001) exhibit a much stronger O_2 outgassing in the subpolar South Atlantic [95.0 Tmol yr^{-1} differences between this study and Gruber et al. (2001)]. However, this difference could roughly cancel out when we integrate the whole Southern Ocean regions, as it also exists a larger O_2 influx in subpolar Indian-Pacific Ocean and Oceans >58°S (differences of −58.1 and −26.2 Tmol yr^{-1}, respectively). Besides, the spatial distribution shows a remarkable consistency with preindustrial experiments presented by Resplandy et al. (2015), indicating the robust of models in simulating O_2 flux.

3.1.2. *Modifications of air-sea O_2 flux under global warming*

Temporal evolution of the air-sea O_2 flux reveals that significant modifications have been occurring in response to ongoing climate change (Fig. 2). In Fig. 2a, we can see sizable oscillations of air-sea O_2 flux during the period 1950–85. Also obvious is the increase of oceanic O_2 outgassing found since the mid-1980s, with an upward trend of ~1.49 Tmol yr^{-2} (significant at 0.01 level). Based on EEMD method, here we split the evolution of air-sea O_2 flux into decadal variability (i.e. sum of IMFs 2–5 from EEMD) and the long-term trend (i.e. IMF 6). As shown in Fig. 2b, the time series of air-sea O_2 flux from 1950 to 1985 is primarily dominated by natural decadal variability, while the human-induced long-term changes gradually wields its influence after 1985. The combination of the two terms eventually lead to an overall upward trend since the 1980s, with natural variability modulating the long-term trend.

The EOF analysis was applied to the de-trended global air-sea O_2 flux over the 1985–2014 period to explore the spatio-temporal distributions of decadal variability (Fig. 3). The first two modes explain approximately 58% of the total variance. The highest decadal variability of O_2 flux is found in the North Pacific, the North Atlantic and the Southern Ocean (Figs. 3a, 3b). The most significant changes in the Atlantic are mainly in the high-latitude areas where the sinking branch of the Atlantic Meridional Overturning Circulation (AMOC) is located, the changes of which could significantly influence climate (Yang et al., 2016; Wen et al., 2018; Yang and Wen, 2020). In the Southern Ocean, the spatial pattern exhibits opposite phase between 40°S and 65°S, suggesting the potential relationship with the Southern Annular Mode (SAM). Time series associated with EOF modes reveal a cycle of ~15 years with different phases in PC1 and PC2 (Fig. 3c). The standard deviation of the decadal variability derived from EEMD also shows a similar spatial distribution compared with the EOF analysis (Fig. S4 in the ESM).

The long-term changes of air-sea O_2 flux, which are generally considered as modifications to anthropogenic forcing, is presented in Fig. 4. Positive values are mainly found in the high latitude areas (Fig. 4a), where strong O_2 uptake in the climatological state is seen (Fig. 1a), revealing the weakening of the oceanic O_2 absorption capacity from the atmosphere. The maximum increase of the flux occurs in the Southern Ocean (SO>58°S), where it reaches 5.39±0.34 Tmol yr^{-1}. The next two highest increases occur in the North Pacific (Temp NPac) and North Atlantic (N NAtl), with an increase about 4.39±0.17 and 3.25±0.11 Tmol yr^{-1}, respectively (Fig. 4b). This long-term change could be attributed to human-induced solubility and circulation changes. The sol-

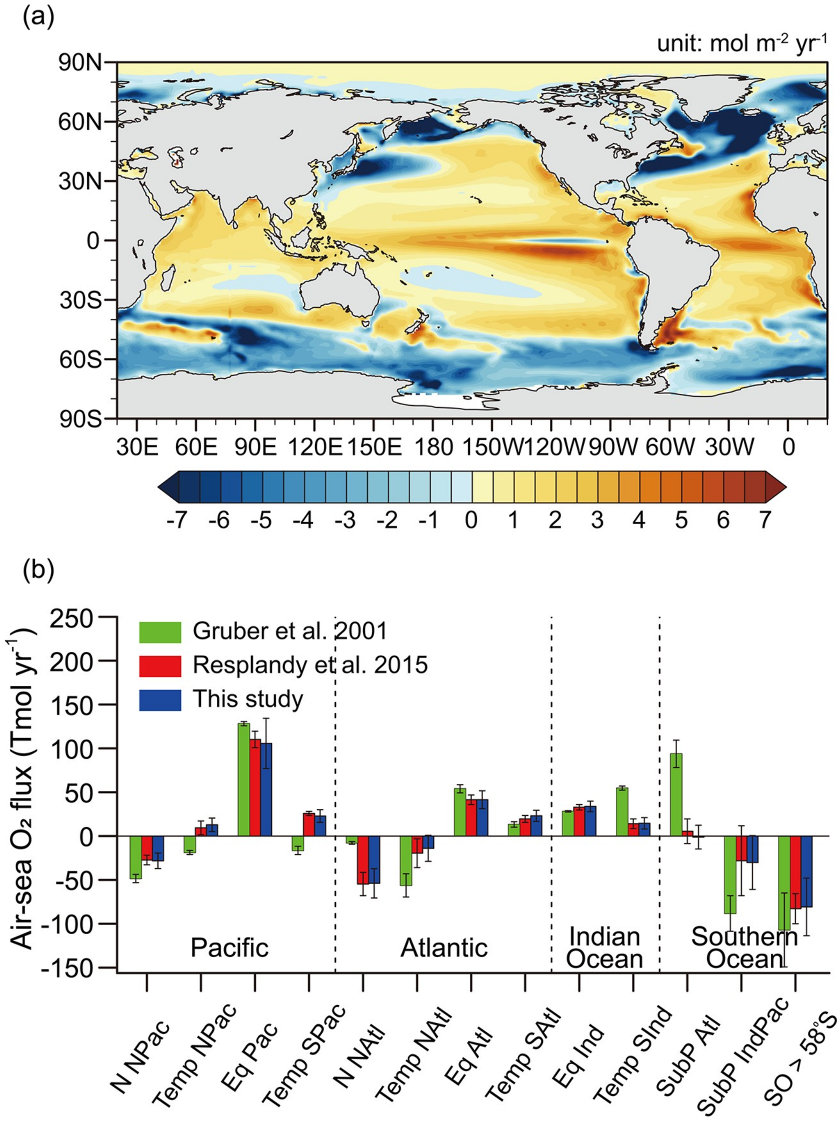

Fig. 1. The spatial distributions of annual mean air-sea O_2 flux (a) averaged from 1985 to 2014 in CMIP6 historical simulations, and (b) compared with two other studies. Positive flux in Fig. 1a means O_2 outgassing from ocean to the atmosphere. For sake of comparisons, the ocean is partitioned into 13 regions as shown in Fig. S3 in the ESM. The results from Li et al (2020) are similar with Resplandy et al 2015, which are not shown here.

ubility of dissolved O_2 has been decreasing in the warming ocean. This effect could be written as:

$$F_{\text{them,air-sea}} = -\frac{Q}{C_p}\frac{\partial O_2}{\partial T}\,, \tag{11}$$

where Q is the total sea-surface downward heat flux; C_p represents the heat capacity of sea water; $\partial O_2/\partial T$ is the temperature dependence of O_2 solubility which could be derived from Garcia and Gordon (1992). Our calculations reveal that roughly one quarter of the increase is directly associated with reduced solubility in the warming ocean, which is consistent with results found by Li et al. (2020) and Plattner et al. (2002). Warming-induced ocean stratification also plays an important role in the modifications of air-sea O_2 flux. Strong shoaling of the mixed layer is found in the North Atlantic and widespread areas in the Southern Ocean (Fig. S5 in the ESM), which prevents oxygen supplies from reaching the deeper layers and eventually result in a positive contribution to the air-sea O_2 flux.

3.1.3. *Comparisons with CMIP5: What's new about the air-sea O_2 flux we can learn in CMIP6*

In Li et al. (2020), the air-sea O_2 flux derived from CMIP5 is applied to investigate the terrestrial and oceanic carbon sinks. It is therefore necessary to clarify the difference of the flux between the CMIP5 and CMIP6 as well as its influences on carbon sink estimations.

For a simulated historical period from 1975 to 2005, the comparisons between CMIP6 (this study) and CMIP5

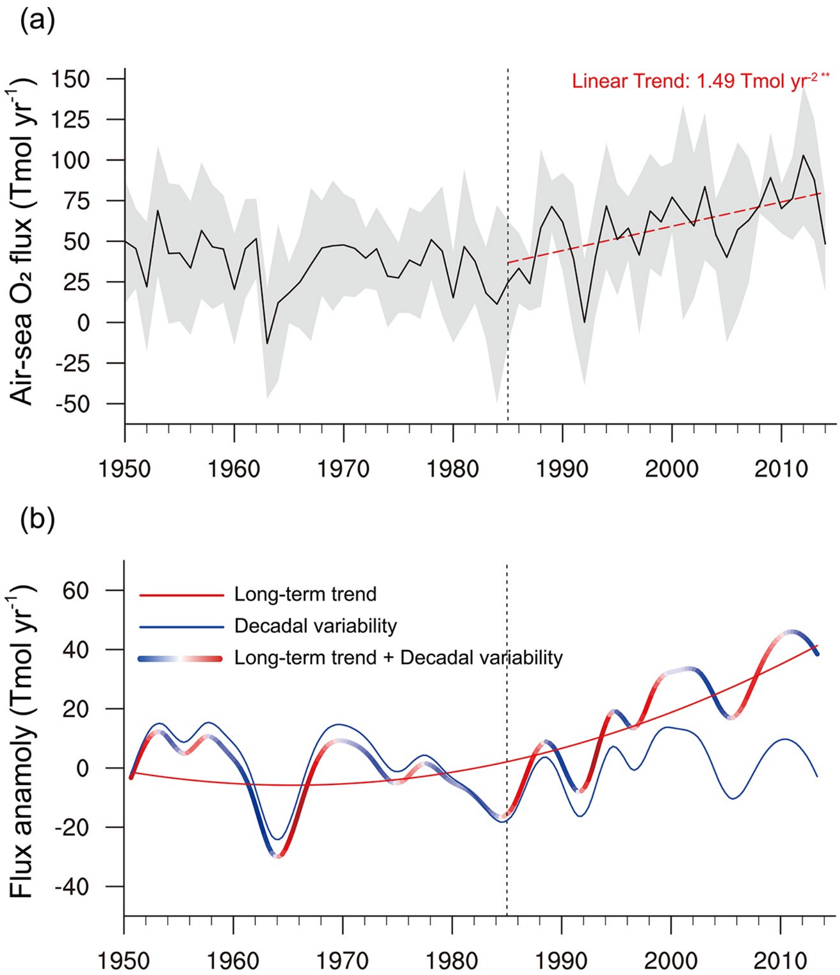

Fig. 2. Time series in the historical period (1950–2014) of (a) air-sea O_2 flux and (b) its EEMD decomposition. The red dashed line in (a) represents linear regression from 1980 to 2014, significant at the 0.01 level. Shaded area is the uncertainty of the flux represented by the standard deviation of these models. The decadal variability in (b) (the blue solid line) is the sum of IMF2-5 from the EEMD and the long-term trend (the red solid line) is the IMF6. Positive values in both panels indicate oceanic O_2 outgassing to the atmosphere.

[derived from Li et al. (2021)] reveal pronounced temporally varying differences of air-sea O_2 flux (Fig. 5). Except for a short period of time around year 1990, the ocean in CMIP6 exhibits an overall smaller oceanic O_2 outgassing, up to −22 Tmol yr^{-1}, than in CMIP5. Spatial patterns shown in Fig. 5b reveal that this difference is mainly caused by the intensified high-latitude oceanic O_2 uptake in CMIP6, especially in the North Atlantic and Southern Ocean. Although there still exists relatively large uncertainties, this intensified uptake in CMIP6 is more consistent with the regional observations in the Southern Ocean (Bushinsky et al., 2017), reflecting the improvement of simulations in CMIP6. Furthermore, slight difference also exists in the long-term trend of air-sea O_2 flux. An upward linear trend of ~1.52 Tmol yr^{-2} has been found in CMIP6 during the period 1985 to 2005, while the trend is approximately 1.12 Tmol yr^{-2} in CMIP5. This indicates an accelerated oceanic O_2 outgassing in CMIP6, which is tightly associated with ocean deoxygenation (Bopp et al., 2013; Palter and Trossman, 2018; Li et al., 2020).

According to Eqs. (6)–(8), this difference in O_2 flux could lead to a total fluctuation as large as 0.4 GtC yr^{-1} in the estimated carbon sink. It should be noted that, besides the air-sea O_2 flux, the estimated carbon sink could also be influenced by the choice of other oxygen datasets in the study, which is therefore rather complicated. Comparisons of O_2-based carbon sinks between this study and Li et al. (2021), as well as other previous studies, will be discussed in detail in the following section.

3.2. *Estimates of terrestrial and oceanic carbon sinks*

3.2.1. *O_2-CO_2 diagram from 1990 to 2014*

Simulations of the air-sea O_2 flux in CMIP6 provide a valuable complement for the O_2-based carbon uptake estimations. With the use of air-sea O_2 flux as well as other O_2-

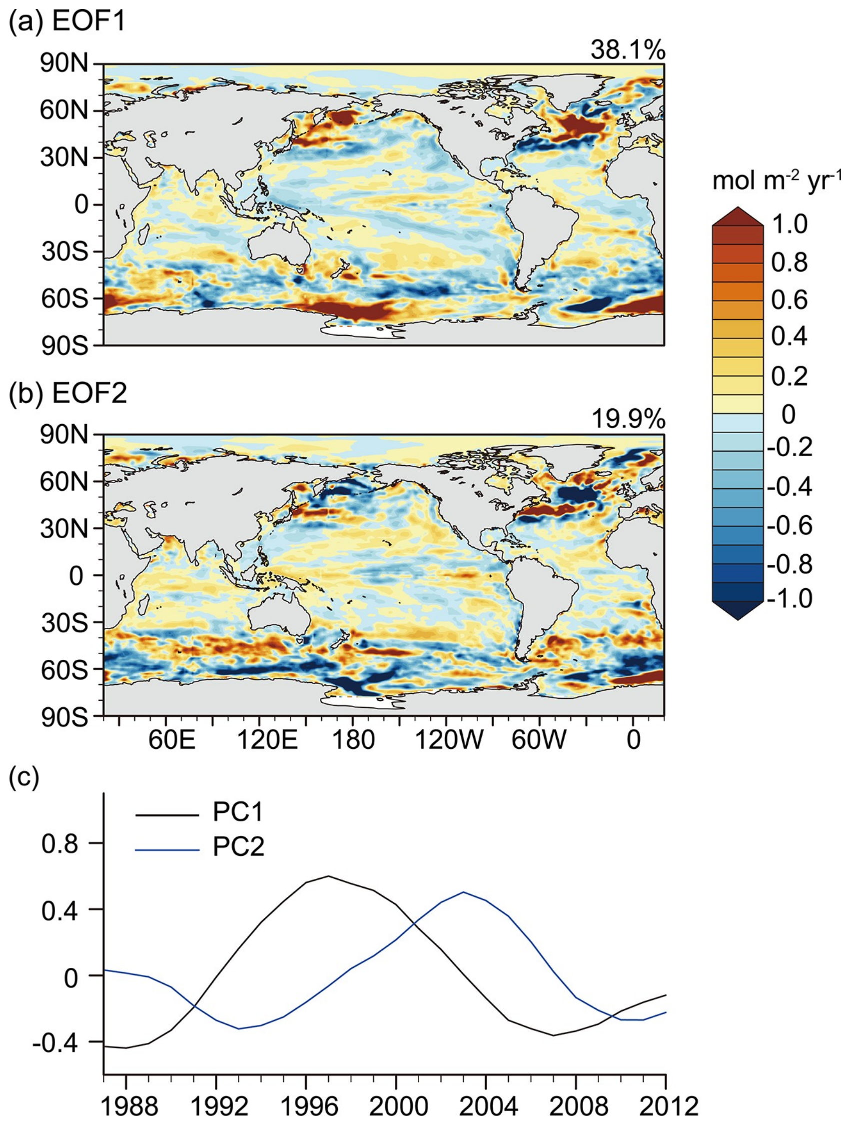

Fig. 3. EOF analysis of de-trended global air-sea O_2 flux over the 1985–2014 period. The spatial patterns of the first and second EOF mode are presented in panel (a) and (b), respectively. The black and blue lines in (a) represent the temporal coefficient of the two modes. Note that the original timeseries is pre-processed with a pentad running average to remove the influence of the high-frequency oscillations.

related variables, the global terrestrial and oceanic carbon sinks could be calculated based on Eqs. (1)–(9). The processes are briefly diagrammed in Fig. 6.

The dots in Fig. 6 are the observed anomalies of global atmospheric CO_2 (horizontal axis) and O_2/N_2 concentrations (vertical axis) from 1990 to 2014. Here we set the concentrations in year 1990 as the base point (0 ppm, 0 per meg). These dots show an increase of CO_2 concentration and a simultaneous decline in O_2/N_2 concentration with time. For example, the concentrations in 2014 could be written as (44 ppm, −465 per meg) in this coordinate system, which means a 44 ppm increase of CO_2 concentration and a 465 per meg decrease of O_2/N_2 concentration in the atmosphere since year 1990. The arrows in Fig. 6 reveal the effect of related processes on atmospheric CO_2 and O_2/N_2 concentration changes. For example, the fossil fuel combustion is marked by the black arrow in Fig. 6, starting at (0, 0) and ending at (89.0, −584.7), meaning that the fossil fuel burning would have contributed to a total 89.0 ppm increase of CO_2 (that is, a release of 189.0 GtC CO_2, 1 Gt = 10^{15} g, 1 ppm = 2.12 GtC) and 584.7 per meg decrease of O_2/N_2 concentration during 1990–2014, if no other processes were involved. This is to say, the observed decline of O_2/N_2 (~465.1 per meg) is a bit smaller compared with the decline directly derived from fossil fuel combustion (584.7 per meg) during 1990–2014. More importantly, the observed atmospheric CO_2 concentration only increases by about half of the value derived from fossil fuel combustion (that is, ~44 ppm, as shown in Fig. 6 and Fig. 7), from which we can thus infer huge land and ocean carbon sinks, absorbing a total of 96.6 GtC carbon. The projections of these arrows on the *x*- axis are also drawn in Fig. 6, which reflect how the atmospheric CO_2 con-

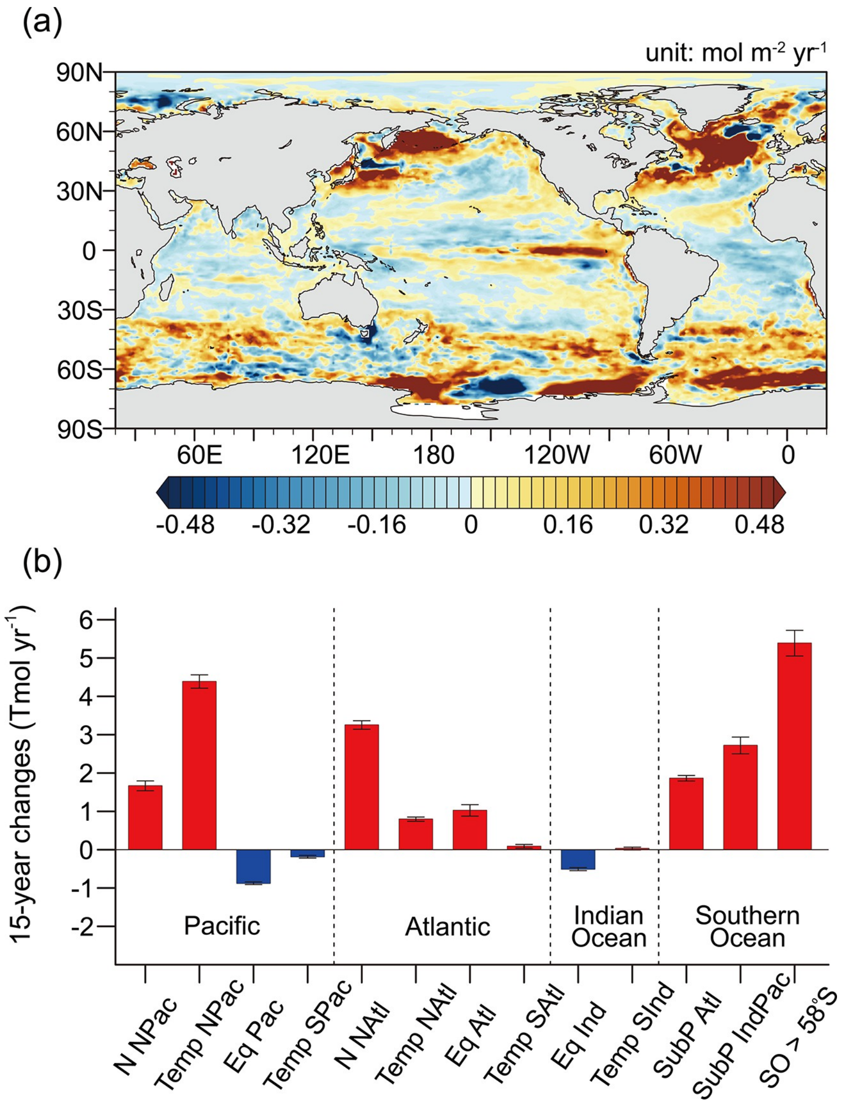

Fig. 4. 15-year changes in the long-term trend of air-sea O_2 flux since 1985. The error bars in panel (b) represent the uncertainty of flux change.

centrations are influenced by the related processes. The land and ocean carbon sinks can be separated from the total carbon uptake according to Eq. (6) and Eq. (7), as 33.5 GtC and 63.2 GtC, respectively, during this period.

It should be especially noted that the air-sea O_2 flux plays an important role in the carbon uptake estimations. The ocean emits ~1.54 Pmol O_2 (1 Pmol = 10^{15} mol) to the atmosphere (sum of the air-sea O_2 flux from 1990 to 2014 in Fig. 2a), making a positive contribution of about 36.7 per meg to the atmospheric O_2/N_2 concentration (red vector in Fig. 6). Despite this air-sea O_2 flux being relatively small, it plays an important role in the estimation of land and ocean carbon sinks. Figure 8 describes the situation assuming that the air-sea O_2 flux is negligible on a multiannual-to-decadal timescale, as proposed in the early studies (Bender and Battle, 1999; Battle et al., 2000). If the air-sea O_2 flux is not considered in the O_2 budget, the ocean carbon sink would be apparently underestimated by approximately 14.8 GtC during 1990–2014, while the land carbon uptake would be largely overestimated (bar charts in the top right of Fig. 8).

3.2.2. *Averaged terrestrial and oceanic carbon sinks in different periods*

We subsequently calculated the averaged terrestrial and oceanic carbon uptake over several different periods and compared them with previous O_2-based carbon uptake estimations (Table 3). Here, we use the linear trend of atmospheric O_2/N_2 and CO_2 concentrations in the period to represent the O_2/N_2 and CO_2 changes in Eqs. (6)–(7) ($\Delta\delta(O_2/N_2)$ and ΔCO_2). For observed atmospheric concentration changes and fossil fuel consumption (F_{fossil}), our results are relatively consistent with Keeling et al. (2014) (differences less than 0.06 ppm yr^{-1} in ΔCO_2 and 0.12 GtC yr^{-1} in F_{fossil}). The effect of air-sea flux in our study (which are derived from process-based CMIP6 model simulations, as described above) shows a relatively large discrepancy with that in Keeling et al. (2014) (which is calculated based on the linear regression between O_2 flux and net changes of ocean heat content). Our results

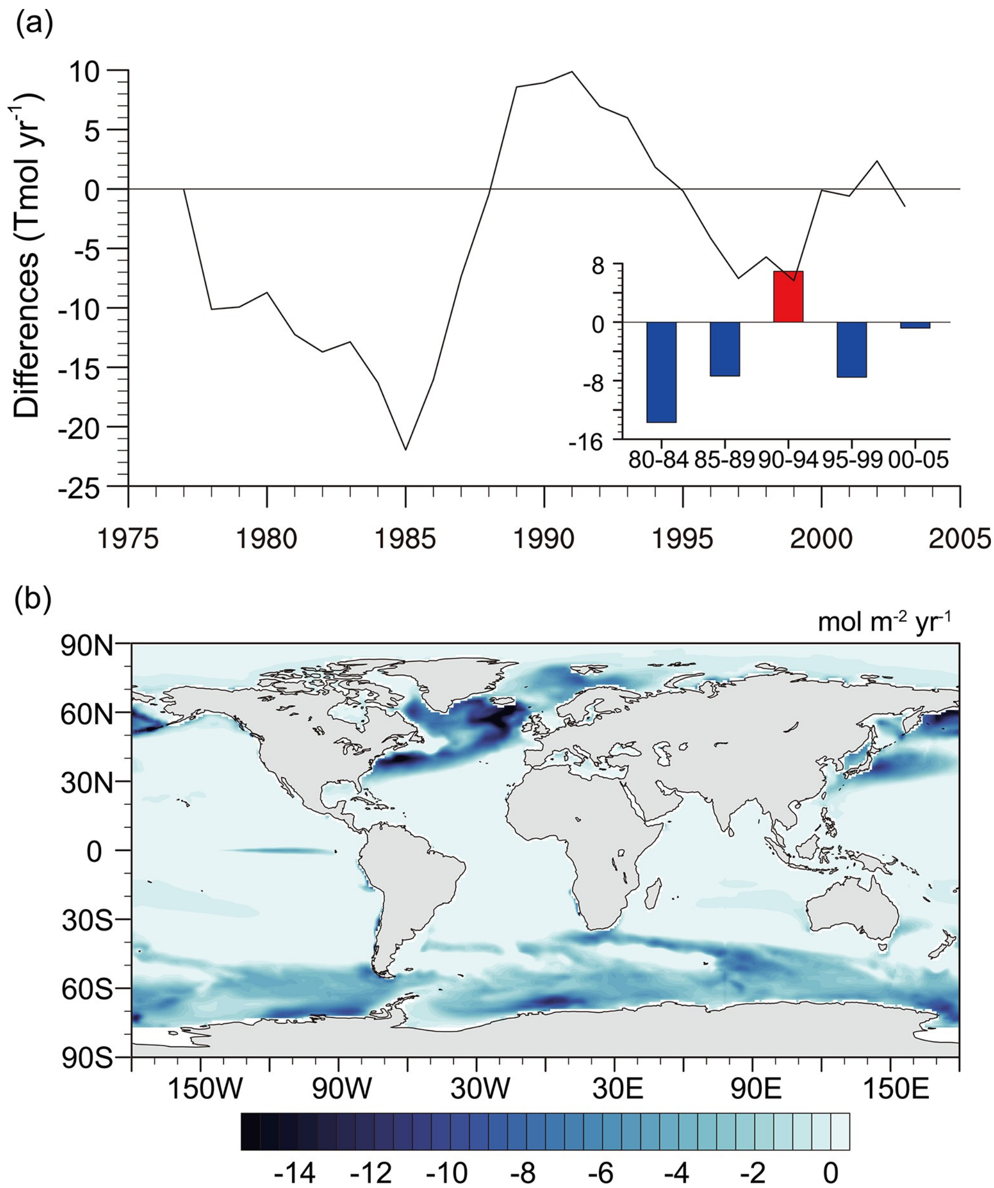

Fig. 5. Differences of air-sea O_2 flux between CMIP6 and CMIP5 during period 1975–2005 (i.e. $FLUX_{CMIP6}$ minus $FLUX_{CMIP5}$). The black line in (a) is the time series of the difference and (b) shows the spatial distribution of the difference averaged from 1975–2005.

show an averaged ocean and land carbon sink of 2.10±0.43 and 1.14±0.52 GtC yr^{-1}, respectively, during 1990–2000. An increase is found in both ocean and land carbon sinks during 2000–10, while results from Keeling et al. (2014) show an increase in ocean sink but a decline in land sink. Furthermore, the averaged carbon sinks from 2004 to 2008 in our study (2.64±0.66 GtC yr^{-1} for ocean and 1.84±0.79 GtC yr^{-1} for land) are generally larger than that in Tohjima et al. (2019) (1.97±0.62 GtC yr^{-1} for ocean and 2.17±0.82 GtC yr^{-1} for land), which could also be partly attributed to the discrepancy in the air-sea flux (Table 3).

To further explore the temporal changes of ocean and land carbon sinks over the past two decades, the averaged ocean and land carbon sinks were calculated for several representative periods: 1991–97, 1994–2000 and 2004–10 were selected for the estimates of averaged ocean sinks; meanwhile, 1994–2000, 2002–08 and 2008–14 were selected for the estimates of averaged land sinks. These results are shown as the asterisks in Fig. 9, accompanied by time-continuous estimations from the Global Carbon Project (GCP, Friedlingstein et al., 2019), Landschützer et al 2016 and Carbon Tracker (CT, Jacobson et al., 2020). The estimates by GCP clearly show a quasi-monotonous increase of the oceanic carbon sink over the past few decades (Fig. 9a, red line). However, the oceanic uptake in our results show a decline from 2.04±0.47 GtC yr^{-1} in 1991–97 to 1.85±0.45 GtC yr^{-1} in 1994–2000. A significant upward trend is subsequently found in the 21st century, with ocean uptake increasing to 2.87±0.47 GtC yr^{-1} in 2004–10. This temporal pattern is generally consistent with results derived from observed sur-

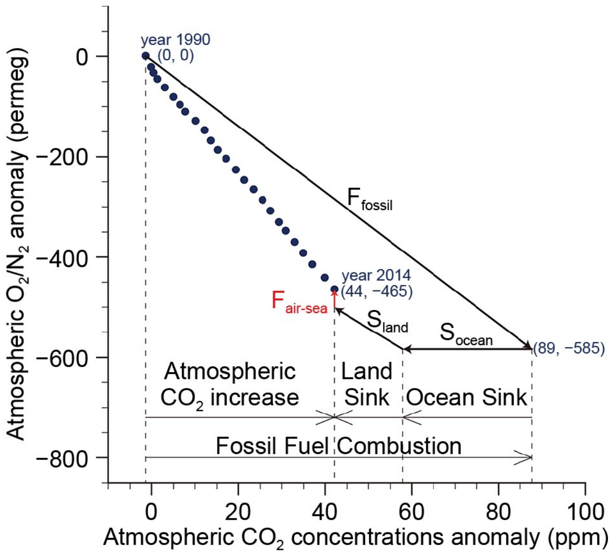

Fig. 6. Changes in observed atmospheric concentrations of O_2/N_2 and CO_2 from 1990 to 2014. The blue dots represent the annual averaged O_2 and CO_2 anomaly (here we choose the concentrations in 1990 as the reference value). The vectors in the diagram schematically illustrate the contribution of each process related to the changes in O_2 (vertical axis) and CO_2 (horizontal axis) during this period. The effect of air-sea O_2 flux is highlighted in red.

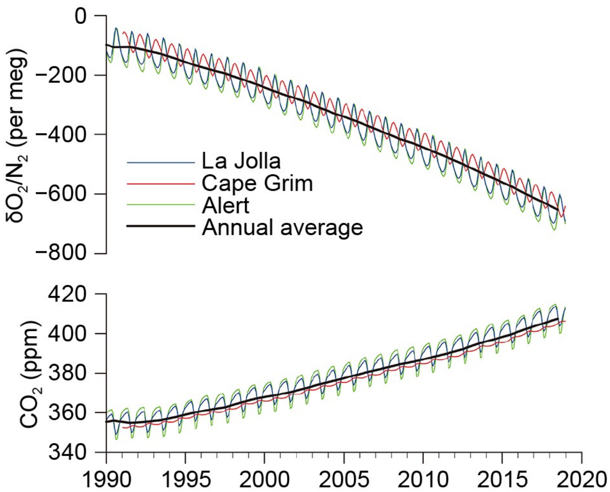

Fig. 7. The observed time series of atmospheric O_2/N_2 and CO_2 concentrations. The blue, green and red lines represents observations in La Jolla (32.9°N, 277.3°W), Alert (82.5°N, 62.3°W), and Cape Grim (40.7°S, 144.7°E), respectively. The black line is the annual mean concentrations averaged among the three stations with a weight of 0.25, 0.25 and 0.5.

face partial pressure of CO_2 in Landschützer et al. (2016) (Fig. 9a, green line), which may occur as consequences of the combined influence of anthropogenic forcing and oceanic internal modes. The net terrestrial carbon uptake estimated in this study corresponds well with the results derived from GCP. An increase of land carbon uptake (from 1.23±0.60 GtC yr^{-1} to 1.91±0.50 GtC yr^{-1} according to our estimations) could be found in the 2000s (Fig. 9b) which

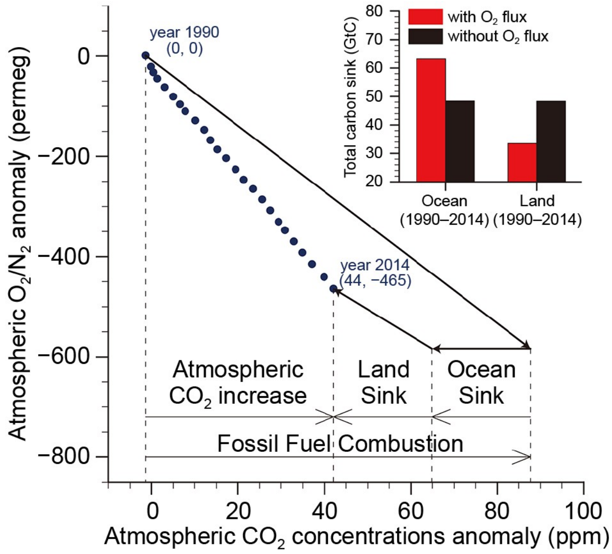

Fig. 8. Role of air-sea O_2 flux in O_2-based carbon sinks estimations. The diagram is same as Fig. 6, except for no air-sea O_2 flux considered in the calculation. The bar charts in the top right show the comparisons between estimated ocean/land carbon sink with and without O_2 flux correction.

has been reported by several atmospheric inversion and model-based studies (Keenan et al., 2016; Ballantyne et al., 2017; Piao et al., 2018). Despite the fact that the mechanisms behind this increase are still under discussion, it is generally believed that the changes in land use, modifications of terrestrial productivity and respiration, as well as climatic variations of temperature and moisture are responsible for changes in terrestrial carbon uptake (Chen et al., 2020; Piao et al., 2020a, b; Yue et al., 2020).

3.2.3. *Influence of oxygen datasets on estimated carbon uptake*

In this section, we specifically investigate the differences of the carbon sinks from that in Li et al. (2021). As mentioned in section 3.1.3, the air-sea O_2 flux used in Li et al. (2021) is derived from CMIP5, while CMIP6 simulation of the flux is used in this study. Meanwhile, the other O_2-related variables (such as atmospheric O_2 decline) in Li et al. (2021) are derived from the oxygen budget proposed by Huang et al. (2018), which is also different from this study. Terrestrial and oceanic carbon uptakes estimated by Li et al. (2021) are depicted by the triangles in Fig. 9. From the comparisons between this study and Li et al. (2021), we can discern the role of oxygen data in carbon sink estimations.

For the terrestrial carbon sink, both of the two studies corresponds well with GCP in the 21st century, which exhibit an enhanced uptake mentioned in section 3.2.2. However, the result from Li et al. (2021) seems to present an unrealistically high land carbon uptake (1.50 GtC yr^{-1}) in the 1990s, while the current study behaves in good agreement with GCP during this period (1.06 GtC yr^{-1}). The oceanic carbon uptake in both this study and Li et al. (2021) exhibits a similar variability with that in Landschützer et al. (2016) (that is, a

Table 3. Estimations of O_2-based carbon sinks in different periods.

	Period	$\Delta\delta$ (O_2/N_2)[a,b] (per meg yr^{-1})	ΔCO_2[a,b] (ppm yr^{-1})	F_{eff}[a,c] (Tmol yr^{-1})	F_{fossil}[a] (GtC yr^{-1})	Ocean sink[a] (GtC yr^{-1})	Land sink[a] (GtC yr^{-1})
Our results	1990–00	−15.81 (0.52)	1.46 (0.08)	45.7 (30.6)	6.37 (0.24)	2.10 (0.43)	1.14 (0.52)
	2000–10	−20.14 (0.34)	1.94 (0.07)	58.7 (31.3)	7.93 (0.83)	2.66 (0.41)	1.15 (0.50)
	2004–08	−19.62 (1.33)	1.79 (0.27)	50.4 (30.1)	8.28 (0.40)	2.64 (0.66)	1.84 (0.79)
Keeling et al., 2014	1990–2000	−15.77	1.52 (0.02)	44 (45)	6.39 (0.38)	1.94 (0.62)	1.22 (0.80)
	2000–10	−20.39	1.90 (0.02)	44 (45)	7.81 (0.47)	2.72 (0.60)	1.05 (0.84)
Tohjima et al., 2019	2004–08	−19.29	1.92 (0.09)	27.5 (27.5)	8.21 (0.41)	1.97 (0.62)	2.17 (0.82)

[a] Estimated uncertainties are shown in parentheses. These uncertainties are propagated to the ocean and land sink uncertainties during calculation. [b] The linear trend of the observations during the selected period. Uncertainties shown in parentheses are the standard error of the regression coefficient. [c] Ensemble mean of the CMIP6 models. Uncertainties shown in parentheses are standard deviation among the models.

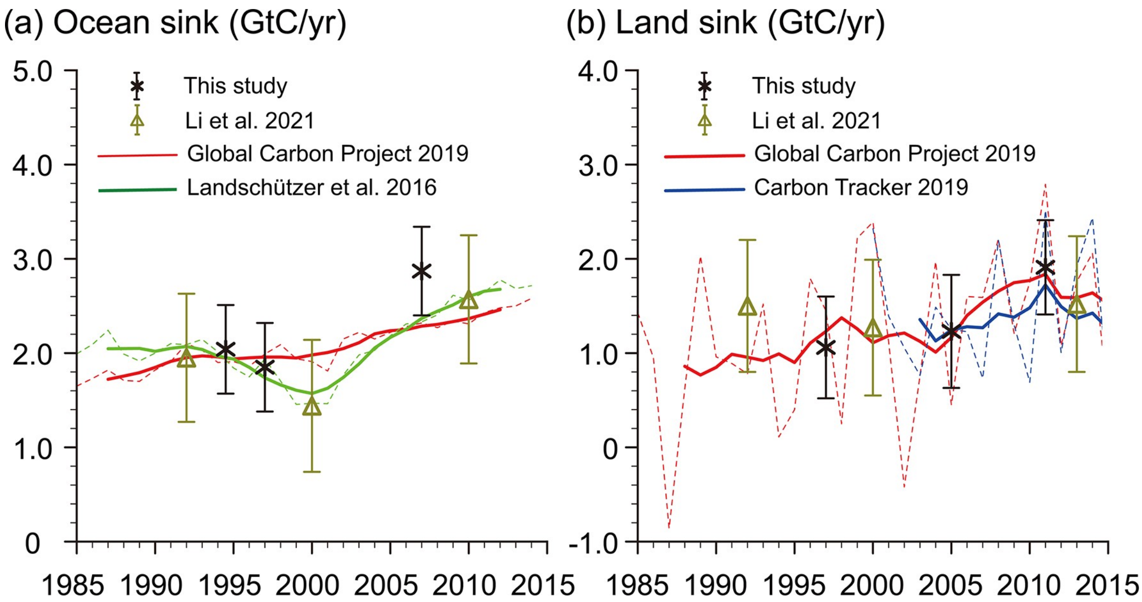

Fig. 9. Estimated ocean and land carbon sinks in different studies. The asterisks and triangles are seven-year averaged carbon sinks in this study and Li et al 2021, with error bars representing uncertainties of the estimations. The time series of carbon sinks derived from Global Carbon Project 2019, Landschützer et al 2016 and Carbon Tracker 2019 are colored in red, green and blue, respectively. The thin dashed lines and the thick solid lines are annual and seven-year running averaged carbon sinks, respectively.

downward trend in the 1990s subsequently followed by an upward trend in the 2000s). Despite this, discrepancy occurs around year 2010, as shown in Fig. 9a. The estimated oceanic carbon uptake in this study (2.87 GtC yr^{-1}) is relatively larger than it in Li et al. (2021) (2.45 GtC yr^{-1}) and GCP (2.36 GtC yr^{-1}).

Overall, both of the two studies reveal an enhanced carbon uptake in the 21st century. This study provides a more reliable estimate of the terrestrial carbon uptake in the 1990s, while the oceanic carbon sink in Li et al. (2021) is more consistent with the Global Carbon Project after year 2010. Our calculations show that the differences in air-sea O_2 flux ($F_{air-sea}$) and atmospheric O_2 change (ΔO_2) are the main contributors to the discrepancies. If the difference in O_2 flux is expressed as $\Delta F_{air-sea}$ (the other variables remain unchanged), its influence on the terrestrial and oceanic carbon uptake could then be respectively expressed as $\Delta B = -\beta/\alpha_B \Delta F_{air-sea}$ and $\Delta O = \beta/\alpha_B \Delta F_{air-sea,}$ according to Equations 6–8. This implies that a weakened oceanic O_2 outgassing, approximately −22 Tmol O_2 yr^{-1}, would lead to an increase of 0.21 GtC yr^{-1} land carbon sink and a simultaneous opposite effect on ocean carbon sink. For the period 1990–95, Li et al. (2021) shows a smaller declining trend of atmospheric O_2 and oceanic outgassing in 1990–95, which could eventually lead to a larger land uptake in Li et al. (2021) during this period. These results highlight the vital importance of oxygen datasets on carbon sink estimations.

4. Summary and discussion

We use the coupled ocean biogeochemistry models in CMIP6 to investigate the modifications of air-sea O_2 flux under climate change and its influences on the estimations of global terrestrial and ocean carbon uptake. Our results show an enhanced global oceanic O_2 outgassing to the atmosphere since the 1980s, accompanied by a strong decadal variability dominated by oceanic internal modes. Consistent with Li et al. (2020), this study shows maximum changes of flux mainly occurring in the high latitudes, with roughly one quarter of the outgassing directly associated with reduced solubility in the warming ocean, and the rest mainly linked with circulation changes and ocean stratification. This modification of air-sea O_2 flux plays an important role in estimating carbon uptake, as described in section 3.2.

The application of air-sea O_2 flux in CMIP6 provides a valuable complement for studies of O_2-based global carbon sinks estimations under climate change. Our results reveal the significant increases of terrestrial and oceanic carbon sinks in the 21st century, reflecting the human impacts on the carbon cycle and Earth's environments. The model biases of air-sea O_2 flux between CMIP5 and CMIP6 are also investigated in this study, which could lead to a total discrepancy up to 0.4 GtC yr^{-1} in the estimations, indicating the importance of improvement of air-sea O_2 flux parameterizations in the model.

Some limitations should also be acknowledged. Our estimation of carbon sinks still suffers from relatively large uncertainties (0.4–0.8 GtC yr^{-1}) due to the accumulations of uncertainty of each term in the calculations. Furthermore, the earliest observations of O_2/N_2 we could obtain are from the late 1980s, which greatly limits the lengths of estimated time series. The comparisons between this study and Li et al. (2021) also reveal the importance of the accuracy of oxygen datasets on the carbon uptake estimations. Presently, we are working on structuring the global oxygen budget (Huang et al., 2018) under the constrain of O_2/N_2 observations, from which we hope to extend the time series of atmospheric O_2 changes back to the 1900s as well as provide a more reliable oxygen dataset. Further explorations and investigations of the O_2-based carbon uptake estimations should be done in the future.

Acknowledgements. The authors acknowledge the Scripps O_2 Program for providing the observations of atmospheric O_2 and CO_2 data. The authors also acknowledge the World Climate Recruitment Programme's (WCRP) Working Group on Coupled Modelling (WGCM), and the Global Organization for Earth System Science Portals (GO-ESSP) for producing outputs of CMIP6 model simulations. This work was jointly supported by the National Science Foundation of China (Grant Nos. 41991231, 91937302) and the China 111 project (Grant No. B13045). The data processes and analysis are supported by Supercomputing Center of Lanzhou University.

Electronic supplementary material: Supplementary material is available in the online version of this article at https://doi.org/10.1007/s00376-021-1273-x.

REFERENCES

Andres, R. J., Boden, T. A. & Marland, G. (2016). Annual fossil-fuel CO2 emissions: Mass of emissions gridded by one degree latitude by one degree longitude. Carbon Dioxide Information Analysis Center, Oak Ridge National Laboratory, U. S. Department of Energy. https://doi.org/10.3334/CDIAC/ffe.ndp058.2016.

Ballantyne, A., and Coauthors, 2017: Accelerating net terrestrial carbon uptake during the warming hiatus due to reduced respiration. *Nature Climate Change*, **7**, 148–152, https://doi.org/10.1038/nclimate3204.

Battle, M., M. L. Bender, P. P. Tans, J. W. C. White, J. T. Ellis, T. Conway, and R. J. Francey, 2000: Global carbon sinks and their variability inferred from atmospheric O_2 and $\delta^{13}C$. *Science*, **287**, 2467–2470, https://doi.org/10.1126/SCIENCE.287.5462.2467.

Battle, M. O., and Coauthors, 2019: Atmospheric measurements of the terrestrial O_2: CO_2 exchange ratio of a midlatitude forest. *Atmospheric Chemistry and Physics*, **19**, 8687–8701, https://doi.org/10.5194/acp-19-8687-2019.

Bender, M. L., and M. O. Battle, 1999: Carbon cycle studies based on the distribution of O_2 in air. *Tellus*, **51**, 165–169, https://doi.org/10.3402/TELLUSB.V51I2.16268.

Bopp, L., C. Le Quéré, M. Heimann, A. C. Manning, and P. Monfray, 2002: Climate-induced oceanic oxygen fluxes: Implications for the contemporary carbon budget. *Global Biogeochemical Cycles*, **16**, 6-1–6-13, https://doi.org/10.1029/2001GB001445.

Bopp, L., and Coauthors, 2013: Multiple stressors of ocean ecosystems in the 21st century: Projections with CMIP5 models. *Biogeosciences*, **10**, 6225–6245, https://doi.org/10.5194/bg-10-6225-2013.

Bushinsky, S. M., A. R. Gray, K. S. Johnson, and J. L. Sarmiento, 2017: Oxygen in the southern ocean from argo floats: Determination of processes driving air-sea fluxes. *J. Geophys. Res.: Oceans*, **122**, 8661–8682, https://doi.org/10.1002/2017JC012923.

Chen, G., and Coauthors, 2020: Global projections of future urban land expansion under shared socioeconomic pathways. *Nature Communications*, **11**, 537, https://doi.org/10.1038/s41467-020-14386-x.

Cheng, L. J., and J. Zhu, 2018: 2017 was the warmest year on record for the global ocean. *Adv. Atmos. Sci.*, **35**, 261–263, https://doi.org/10.1007/s00376-018-8011-z.

Cheng, L. J., G. J. Wang, J. P. Abraham, and G. Huang, 2018: Decadal ocean heat redistribution since the late 1990s and its association with key climate modes. *Climate*, **6**, 91, https://doi.org/10.3390/cli6040091.

Cheng, L. J., K. E. Trenberth, J. Fasullo, T. Boyer, J. Abraham, and J. Zhu, 2017: Improved estimates of ocean heat content from 1960 to 2015. *Science Advances*, **3**, e1601545, https://doi.org/10.1126/SCIADV.1601545.

Dai, M., and Coauthors, 2013: Why are some marginal seas sources of atmospheric CO_2? *Geophys. Res. Lett.*, **40**, 2154–2158, https://doi.org/10.1002/grl.50390.

DeVries, T., and Coauthors, 2019: Decadal trends in the ocean carbon sink. *Proceedings of the National Academy of Sciences of the United States of America*, **116**, 11 646–11 651, https://doi.org/10.1073/PNAS.1900371116.

Dhanda, K. K., and L. P. Hartman, 2011: The ethics of carbon neutrality: A critical examination of voluntary carbon offset providers. *Journal of Business Ethics*, **100**, 119–149, https://doi.org/10.1007/s10551-011-0766-4.

Friedlingstein, P., and Coauthors, 2019: Global carbon budget 2019. *Earth System Science Data*, **11**, 1783–1838, https://doi.org/10.5194/essd-11-1783-2019.

Frölicher, T. L., E. M. Fischer, and N. Gruber, 2018: Marine heatwaves under global warming. *Nature*, **560**, 360–364, https://doi.org/10.1038/s41586-018-0383-9.

Gao, Z. M., H. P. Liu, E. Arntzen, D. P. Mcfarland, X. Y. Chen, and M. Y. Huang, 2020: Uncertainties in turbulent statistics and fluxes of CO_2 associated with density effect corrections. *Geophys. Res. Lett.*, **47**, e2020GL088859, https://doi.org/10.1029/2020GL088859.

Gao, Z. M., H. P. Liu, J. E. C. Missik, J. Y. Yao, M. Y. Huang, X. Y. Chen, E. Arntzen, and D. P. McFarland, 2019: Mechanistic links between underestimated CO_2 fluxes and non-closure of the surface energy balance in a semi-arid sagebrush ecosystem. *Environmental Research Letters*, **14**, 044016, https://doi.org/10.1088/1748-9326/ab082d.

Garcia, H. E., and L. I. Gordon, 1992: Oxygen solubility in seawater: Better fitting equations. *Limnology and Oceanography*, **37**, 1307–1312, https://doi.org/10.4319/lo.1992.37.6.1307.

Gruber, N., M. Gloor, S. M. Fan, and J. L. Sarmiento, 2001: Air-sea flux of oxygen estimated from bulk data: Implications for the marine and atmospheric oxygen cycles. *Global Biogeochemical Cycles*, **15**, 783–803, https://doi.org/10.1029/2000GB001302.

Han, D. L., J. P. Huang, L. Ding, X. Y. Liu, C. Y. Li, and F. Yang, 2021: Oxygen footprint: An indicator of the anthropogenic ecosystem changes. *Catena*, **206**, 105501, https://doi.org/10.1016/j.catena.2021.105501.

Huang, J. P., H. P. Yu, X. D. Guan, G. Y. Wang, and R. X. Guo, 2016: Accelerated dryland expansion under climate change. *Nature Climate Change*, **6**, 166–171, https://doi.org/10.1038/NCLIMATE2837.

Huang, J. P., Y. K. Xie, X. D. Guan, D. D. Li, and F. Ji, 2017a: The dynamics of the warming hiatus over the Northern Hemisphere. *Climate Dyn.*, **48**, 429–446, https://doi.org/10.1007/s00382-016-3085-8.

Huang, J. P., H. P. Yu, A. G. Dai, Y. Wei, and L. T. Kang, 2017b: Drylands face potential threat under 2°C global warming target. *Nature Climate Change*, **7**, 417–422, https://doi.org/10.1038/NCLIMATE3275.

Huang, J. P., J. P. Huang, X. Y. Liu, C. Y. Li, L. Ding, and H. P. Yu, 2018: The global oxygen budget and its future projection. *Science Bulletin*, **63**, 1180–1186, https://doi.org/10.1016/j.scib.2018.07.023.

Huang, J. P., and Coauthors, 2021: The oxygen cycle and a habitable Earth. *Science China Earth Sciences*, **64**, 511–528, https://doi.org/10.1007/s11430-020-9747-1.

Jacobson, A. R., and Coauthors, 2020: CarbonTracker CT2019. Available from https://doi.org/10.25925/39m3-6069.

Ji, F., Z. H. Wu, J. P. Huang, and E. P. Chassignet, 2014: Evolution of land surface air temperature trend. *Nature Climate Change*, **4**, 462–466, https://doi.org/10.1038/nclimate2223.

Keeling, R. F., and S. R. Shertz, 1992: Seasonal and interannual variations in atmospheric oxygen and implications for the global carbon cycle. *Nature*, **358**, 723–727, https://doi.org/10.1038/358723a0.

Keeling, R. F., and A. C. Manning, 2014: Studies of recent changes in atmospheric O_2 content. *Treatise on Geochemistry*. vol 5. 2nd ed., H. D. Holland and K. K. Turekian, Eds., Elsevier, 385–404, https://doi.org/10.1016/B978-0-08-095975-7.00420-4.

Keenan, T. F., I. C. Prentice, J. G. Canadell, C. A. Williams, H. Wang, M. Raupach, and G. J. Collatz, 2016: Recent pause in the growth rate of atmospheric CO_2 due to enhanced terrestrial carbon uptake. *Nature Communications*, **7**, 13428, https://doi.org/10.1038/ncomms13428.

Landschützer, P., N. Gruber, and D. C. E. Bakker, 2016: Decadal variations and trends of the global ocean carbon sink. *Global Biogeochemical Cycles*, **30**, 1396–1417, https://doi.org/10.1002/2015GB005359.

Laszuk, D., 2017. Python implementation of Empirical Mode Decomposition algorithm.GitHub. https://github.com/laszukdawid/PyEMD. GitHub Repository

Li, C. Y., J. P. Huang, Y. L. He, D. D. Li, and L. Ding, 2019: Atmospheric warming slowdown during 1998–2013 associated with increasing ocean heat content. *Adv. Atmos. Sci.*, **36**, 1188–1202, https://doi.org/10.1007/s00376-019-8281-0.

Li, C. Y., J. P. Huang, L. Ding, X. Y. Liu, H. P. Yu, and J. P. Huang, 2020: Increasing escape of oxygen from oceans under climate change. *Geophys. Res. Lett.*, **47**, e2019GL086345, https://doi.org/10.1029/2019GL086345.

Li, C. Y., J. P. Huang, L. Ding, X. Y. Liu, D. L. Han, and J. P. Huang, 2021: Estimation of oceanic and land carbon sinks based on the most recent oxygen budget. *Earth's Future*, **9**, e2021EF002124, https://doi.org/10.1029/2021ef002124.

Liang, J. H., C. Deutsch, J. C. McWilliams, B. Baschek, P. P. Sullivan, and D. Chiba, 2013: Parameterizing bubble-mediated air-sea gas exchange and its effect on ocean ventilation. *Global Biogeochemical Cycles*, **27**, 894–905, https://doi.org/10.1002/gbc.20080.

Liu, X. Y., J. P. Huang, J. P. Huang, C. Y. Li, L. Ding, and W. J. Meng, 2020: Estimation of gridded atmospheric oxygen consumption from 1975 to 2018. *Journal of Meteorological Research*, **34**, 646–658, https://doi.org/10.1007/S13351-020-9133-7.

Manning, A., and R. F. Keeling, 2006: Global oceanic and land biotic carbon sinks from the scripps atmospheric oxygen flask sampling network. *Tellus*, **58**, 95–116, https://doi.org/10.1111/J.1600-0889.2006.00175.X.

Niu, D. X., G. Q. Wu, Z. S. Ji, D. Y. Wang, Y. Y. Li, and T. Gao, 2021: Evaluation of provincial carbon neutrality capacity of china based on combined weight and improved topsis model. *Sustainability*, **13**, 2777, https://doi.org/10.3390/su13052777.

Palter, J. B., and D. S. Trossman, 2018: The sensitivity of future ocean oxygen to changes in ocean circulation. *Global Biogeochemical Cycles*, **32**, 738–751, https://doi.org/10.1002/2017GB005777.

Piao, S., and Coauthors, 2018: Lower land-use emissions responsible for increased net land carbon sink during the slow warming period. *Nature Geoscience*, **11**, 739–743, https://doi.org/10.1038/s41561-018-0204-7.

Piao, S. L., and Coauthors, 2020a: Characteristics, drivers and feedbacks of global greening. *Nature Reviews Earth & Environment*, **1**, 14–27, https://doi.org/10.1038/s43017-019-0001-x.

Piao, S. L., and Coauthors, 2020b: Interannual variation of terrestrial carbon cycle: Issues and perspectives. *Global Change Biology*, **26**, 300–318, https://doi.org/10.1111/gcb.14884.

Plattner, G. K., F. Joos, and T. F. Stocker, 2002: Revision of the global carbon budget due to changing air-sea oxygen fluxes. *Global Biogeochemical Cycles*, **16**, 1096, https://doi.org/10.1029/2001GB001746.

Randerson, J. T., C. A. Masiello, C. J. Still, T. Rahn, H. Poorter, and C. B. Field, 2006: Is carbon within the global terrestrial biosphere becoming more oxidized. *Implications for trends in atmospheric O_2*. *Global Change Biology*, **12**, 260–271, https://doi.org/10.1111/j.1365-2486.2006.01099.x.

Resplandy, L., R. Séférian, and L. Bopp, 2015: Natural variability of CO_2 and O_2 fluxes: What can we learn from centuries-long climate models simulations? *J. Geophys. Res.: Oceans*, **120**, 384–404, https://doi.org/10.1002/2014jc010463.

Seneviratne, S. I., M. G. Donat, A. J. Pitman, R. Knutti, and R. L. Wilby, 2016: Allowable CO_2 emissions based on regional and impact-related climate targets. *Nature*, **529**, 477–483, https://doi.org/10.1038/nature16542.

Tohjima, Y., H. Mukai, T. MacHida, Y. Hoshina, and S. I. Nakaoka, 2019: Global carbon budgets estimated from atmospheric O_2N_2 and CO_2 observations in the western Pacific region over a 15-year period. *Atmospheric Chemistry and Physics*, **19**, 9269–9285, https://doi.org/10.5194/acp-19-9269-2019.

Trenberth, K. E., J. T. Fasullo, and M. A. Balmaseda, 2014: Earth' s energy imbalance. *J. Climate*, **27**, 3129–3144, https://doi.org/10.1175/JCLI-D-13-00294.1.

Wanninkhof, R., 1992: Relationship between wind speed and gas exchange over the ocean. *J. Geophys. Res.: Oceans*, **97**, 7373–7382, https://doi.org/10.1029/92JC00188.

Wei, Y., J. G. Wu, J. P. Huang, X. Y. Liu, D. L. Han, L. L. An, H. P. Yu, and J. P. Huang, 2021: Declining oxygen level as an emerging concern to global cities. *Environ. Sci. Technol.*, **55**, 7808–7817, https://doi.org/10.1021/acs.est.1c00553.

Wen, Q., J. Yao, K. Döös, and H. J. Yang, 2018: Decoding hosing and heating effects on global temperature and meridional circulations in a warming climate. *J. Climate*, **31**, 9605–9623, https://doi.org/10.1175/JCLI-D-18-0297.1.

Willis, J. K., D. Roemmich, and B. Cornuelle, 2004: Interannual variability in upper ocean heat content, temperature, and thermosteric expansion on global scales. *J. Geophys. Res.: Oceans*, **109**, C12036, https://doi.org/10.1029/2003JC002260.

Yang, B., S. R. Emerson, and S. M. Bushinsky, 2017: Annual net community production in the subtropical Pacific Ocean from in situ oxygen measurements on profiling floats. *Global Biogeochemical Cycles*, **31**, 728–744, https://doi.org/10.1002/2016GB005545.

Yang, H. J., and Q. Wen, 2020: Investigating the role of the Tibetan Plateau in the formation of atlantic meridional overturning circulation. *J. Climate*, **33**, 3585–3601, https://doi.org/10.1175/JCLI-D-19-0205.1.

Yang, H. J., K. Wang, H. J. Dai, Y. X. Wang, and Q. Li, 2016: Wind effect on the Atlantic meridional overturning circulation via sea ice and vertical diffusion. *Climate Dyn.*, **46**, 3387–3403, https://doi.org/10.1007/s00382-015-2774-z.

Yue, C., P. Ciais, R. A. Houghton, and A. A. Nassikas, 2020: Contribution of land use to the interannual variability of the land carbon cycle. *Nature Communications*, **11**, 3170, https://doi.org/10.1038/s41467-020-16953-8.